Journal of the Mechanics and Physics of Solids 58 (2010) 330–345

Contents lists available at ScienceDirect

Journal of the Mechanics and Physics of Solids

journal homepage: www.elsevier.com/locate/jmps

The influence of mechanical strain on the optical properties of spherical gold nanoparticles

Xiaohu Qian, Harold S. Park *

Department of Mechanical Engineering, University of Colorado, Boulder, CO 80309, USA

ARTICLE INFO

Article history:
Received 23 July 2009
Received in revised form
3 December 2009
Accepted 6 December 2009

Keywords:
Gold nanoparticles
Localized surface plasmon resonance
Mie scattering theory
Optomechanical coupling
Surface enhanced Raman scattering

ABSTRACT

We utilize classical Mie scattering theory to investigate the effects of tensile and compressive mechanical strain on both the far field (absorption, scattering and extinction efficiencies) and near field (surface enhanced Raman scattering) optical properties of spherical gold nanoparticles with diameters ranging from 10 to 100 nm. By accounting for the strain effects on both the ionic core (bound) and conduction (free) electrons through appropriate modifications of the bulk dielectric functions, we find that gold nanoparticles are relatively sensitive to the effects of mechanical strain due to the fact that the plasmon resonance wavelength for spherical gold particles, which occurs around $\lambda = 520$ nm, is nearly coincident with the interband transitions of the core electrons. Specifically, we find that tensile strain leads to significant enhancements ranging from 60% to 120% in the far field optical efficiencies, while compressive strain leads to similar decreases, and that the plasmon resonance wavelength can be red or blueshifted up to 100 nm due to the applied strain. Finally, we find that tensile strain also strongly enhances the local electric (E)-field at the surface of the nanoparticles, which is of considerable interest for surface-enhanced Raman scattering applications; 5% tensile strain is found to enhance the $|E|^4$ intensity by 63%. The present results demonstrate the potential of mechanical strain, and specifically that of tensile mechanical strain in enhancing and tailoring the optical properties of gold nanoparticles.

1. Introduction

The optical properties of FCC metal (gold and silver) nanostructures have recently been the focus of intense scientific study. One major reason for this is because upon interaction with incident electromagnetic waves such as light, these metal nanostructures exhibit localized surface plasmon resonance (LSPR) (Ozbay, 2006; Sambles et al., 1991; Barnes et al., 2003). Surface plasmons can be thought of as light waves that become trapped along the surfaces of the metal due to interactions with the free, or conduction electrons of the metal. In response, the conduction electrons of the metal may oscillate in resonance with the light waves at specific incident frequencies, which depend upon the material properties of the metal. The specific wavelength at which the resonance occurs is known as the plasmon resonance wavelength, which manifests itself physically through light emission at distinct wavelengths of light in the visible spectrum for gold ($\lambda = 520$ nm) nanoparticles, and in the ultraviolet for silver ($\lambda = 380$ nm) nanoparticles. Many excellent review articles have been written in the past decade which both summarize the fundamentals of LSPR as well as potential applications (Link and El-Sayed, 1999b; Barnes et al., 2003; Sambles et al., 1991; Kelly et al., 2003).

* Corresponding author.
E-mail address: harold.park@colorado.edu (H.S. Park).

0022-5096/$ - see front matter © 2009 Elsevier Ltd All rights reserved.
doi:10.1016/j.jmps.2009.12.001

A key development that has greatly aided the understanding of nanostructure LSPR has been the recent progress in nanostructure synthesis. Many groups have demonstrated through various growth and synthesis techniques that metal nanostructures of diverse and controlled shapes, sizes, and geometries can now be experimentally synthesized (Sun and Xia, 2003; Murphy and Jana, 2002). In doing so, researchers have determined, both through theory and experiment, that the optical properties of metal nanostructures have a strong dependence on the nanostructure size and shape (Kelly et al., 2003; Link and El-Sayed, 1999b; Lee and El-Sayed, 2005; Bryant et al., 2008; Felidj et al., 1999; Hao and Schatz, 2004).

The fact that metal nanostructures exhibit LSPR has led to a plethora of potential applications in all areas of nanoscience. One critical application for metal nanostructures is that of molecular sensing and detection, which is based upon the surface-enhanced Raman scattering (SERS) of metal nanostructures; the physical mechanism for SERS is a substantial enhancement of the local electric field at the nanostructure surface by two or three orders of magnitude. Due to SERS, the increases in local electric field intensity can lead to Raman enhancements of up to $10^{12}-10^{13}$ in the case of interacting metallic nanoparticles (Hao and Schatz, 2004; Kneipp et al., 2006). These dramatic Raman enhancements are important as they indicate that the nanoparticles can be utilized for single molecule sensing and detection (Oldenburg et al., 1998; Sun and Xia, 2003; Barnes et al., 2003; Anker et al., 2008). Other potential applications for SPR nanostructures include nanooptics and plasmonics, in which light can be concentrated and propagated using subwavelength structures leading to miniaturized photonic devices (Brongersma et al., 2000; Maier et al., 2001; Ozbay, 2006).

However, beyond SERS and single molecule detection, there are a wealth of potential applications that depend upon specific components of the LSPR. In particular, this can be understood from the viewpoint that any incident light upon the nanostructure will be both absorbed and scattered by the nanostructure. The optical extinction, which is the measure of the LSPR that is most often presented both experimentally and theoretically, is simply the summation of the absorption and scattering.

For certain applications, having metal nanostructures that strongly absorb light is of significant interest; this is because when light is absorbed by the nanostructure, the nanostructure releases the energy by dissipating it locally as heat. Therefore, researchers have utilized strongly absorbing metal nanostructures for a variety of applications, in particular localized photothermal ablation treatments for cancer (Hirsch et al., 2003, 2006; Huang et al., 2006). In the experiments by Hirsch et al. (2003), metal nanoshells that are composed of a silica core and a gold shell were exposed to near infrared light. Due to the strong absorption properties of the nanoshell, the light was converted by the nanoshells into heat; the experiments demonstrated that the nanoshells were able to generate a sufficiently large local temperature rise, on the order of 40 °C, which caused the death of tumorous tissue in mice. Other researchers (Sershen et al., 2002) demonstrated that strongly absorbing metal nanoshells could be used for specific optomechanical applications involving thermally stimulated hydrogels.

Conversely, the ability of the metal nanostructure to strongly scatter light is critical for optical sensing, tagging and imaging applications (Raschke et al., 2004; Malinsky et al., 2001). Applications involving light scattering are numerous, and include using metal nanostructures as contrast agents in cancer cell imaging (Sokolov et al., 2003; El-Sayed et al., 2005), using composite metal nanostructures for optical labeling and tagging applications (Mock et al., 2002; Nicewarner-Pena et al., 2001), and using metal nanostructures as an optically active strain sensor (Stone et al., 2007). Furthermore, it is important to note that the relative contributions of absorption and scattering to the overall extinction spectra is a function of the nanoparticle size; for example, Jain et al. (2006) showed using classical electrodynamic calculations that the extinction spectra of small gold nanoparticles, with diameters less than about 50 nm, is dominated by absorption, while scattering becomes increasingly important for larger diameters.

The key point of the preceding discussion is that because the specific optical properties of the metal nanostructure, i.e. absorption, scattering and the local electric field, are size-dependent and therefore dictate the applications that the nanostructure can be utilized for, it is of considerable interest to investigate methods by which the far field spectra and local electric field can be enhanced, and to see how the enhancements perform as a function of nanostructure size. It is also important to find new methods of controllably tuning the plasmon resonance wavelength, as such flexibility is demanded by the plethora of previously discussed potential optical applications (Hirsch et al., 2006). Because of this, the purpose of the present work is to utilize analytic Mie scattering theory (Mie, 1908) to investigate a new approach to optical engineering, that of mechanical strain, for spherical gold nanoparticles.

It is relevant to note that the effects of mechanical strain on the electrical and optical properties of both bulk and nanostructured semiconductors (Pistol et al., 1995; Johnson et al., 1998; Audoit et al., 2005; Jiang and Singh, 1997; Lyons et al., 2002; Alizadeh et al., 2004) and more recently carbon nanotubes (Heyd et al., 1997; Liu et al., 2004; Qian et al., 2008) have been recognized and thus studied for some time.

In contrast, to our knowledge, similar systematic investigations for the coupling of mechanics and optics with regards to metal nanostructures have not been performed. In particular, the only effect of strain on the optical properties of metal nanostructures that we are aware of having been studied is that of lattice contraction that is induced by surface stresses (Cammarata, 1994) in ultrasmall (diameter <5 nm) metal nanoparticles (Lerme et al., 2001; Cai et al., 2001; Kreibig and Genzel, 1985; Dalacu and Martinu, 2001; Park et al., 2005). Therefore, generic strain effects that may arise in metal nanostructures due to being embedded in different solid or gaseous media (Kresin, 1995; Fedrigo et al., 1993), increases (Liebsch, 1993) or decreases in temperature (Cai et al., 2001), or simply through applied external force, deformation or pressure, and the resulting effects on the metal nanostructure optical properties have not been accounted for or quantified.

The effects of tensile and compressive strain are accounted for through modifications to both the ionic core (bound) and conduction (free) electron dielectric functions; we also account for surface damping effects that arise from the reduced mean free path of electrons in volume confined nanoparticles. In doing so, our analysis focuses upon three effects. First, we quantify the effect of strain in shifting the plasmon resonance wavelength as compared to an unstrained nanoparticle. Second, we quantify whether strain is an efficient technique to enhance the scattering and absorption efficiencies. Third, we quantify the effects of strain on the local electric field, and thus the SERS enhancements of the nanoparticles. All of these studies are conducted for spherical gold nanoparticles with diameters ranging from 10 to 100 nm to quantify the effectiveness of strain in tuning the optical properties of gold nanoparticles with sizes that are commonly used in modern LSPR and SERS applications.

2. Modifications of the dielectric function

2.1. Surface damping effects

In classical electrodynamic theory, the dielectric function of a material is independent of size. The bulk dielectric function is often expressed as a combination of two terms (Bohren and Huffman, 1983), a Drude–Sommerfeld model for the free or conduction electrons, and a core term representing the bound electrons as

$$\varepsilon_{bulk}(\omega)=\varepsilon_{core}(\omega)+\varepsilon_{free}(\omega)-1, \tag{1}$$

where the free electron term $\varepsilon_{free}(\omega)$ is written as

$$\varepsilon_{free}(\omega)=1-\frac{\omega_p^2}{\omega^2+i\gamma\omega}, \tag{2}$$

and where the plasma frequency $\omega_p=(ne^2/\varepsilon_0 m_{eff})^{1/2}$ depends upon the electron density n and effective mass m_{eff}, and γ is the bulk damping constant, which is related to electron scattering processes. We note that in solid state theory, ε_{core} and ε_{free} originate from interband and intraband transitions, respectively (Palik, 1985).

However, when the size of the nanostructure becomes less than the mean free path of the conduction electrons at around 30–50 nm, the dielectric constant has been experimentally observed to deviate from the bulk value (Coronado and Schatz, 2003; Link and El-Sayed, 1999b; Hovel et al., 1993). The damping constant γ_0, which is the inverse of the collision time for conduction electrons, increases because of the enhanced collision rate with the nanostructure surfaces. The size-dependence of the damping constant can then be written as

$$\gamma(L_{eff})=\gamma_0+A\frac{v_F}{L_{eff}}, \tag{3}$$

where A is a dimensionless parameter whose value is typically less than one, v_F is the Fermi velocity, and $\gamma_0=v_F/l_\infty$, where l_∞ is the mean free path of the conduction electrons in the corresponding bulk material and L_{eff} is the reduced effective mean free path. The parameters utilized in the present calculations for gold are summarized in Table 1; the modifications are performed on the bulk dielectric functions for gold given by Johnson and Christy (1972).

Coronado and Schatz (2003) have developed a geometric probability approach to calculate L_{eff} for arbitrarily shaped convex nanostructures, resulting in the analytic expression

$$L_{eff}=4\frac{V}{S}, \tag{4}$$

where S is the surface area, and V is the volume of the nanostructure. The damping that occurs due to the reduced mean free path is assumed to act solely on the conduction electrons; therefore, the modified bulk dielectric constant in (1) is written as (Hovel et al., 1993; Coronado and Schatz, 2003)

$$\varepsilon_{bulk}(\omega)=\varepsilon_{core}(\omega)-\frac{\omega_p^2}{\omega^2+i\omega\left(\gamma_0+A\frac{v_F}{L_{eff}}\right)}. \tag{5}$$

Table 1
Summary of parameters for gold utilized for surface damping method of Coronado and Schatz (2003).

Material	A	v_F	$1/\gamma_0$	m_{eff}
Gold	0.13	1.41×10^6 m/s	9.3×10^{-15} s	0.99 $m_{electron}$

Value of A taken from Qiu et al. (2008), value for v_F taken from Kittel and McEuen (2004), value for $1/\gamma_0$ and m_{eff} taken from Johnson and Christy (1972).

2.2. Strain effects

In addition to surface damping, we now present the formalism by which the effects of mechanical strain are accounted for on the dielectric function of both the core (bound) and conduction (free) electrons. For the conduction electrons, we follow the work of Cai et al. (2001), who noted that due to strain, the plasma frequency ω_p in (2) changes due to the resulting change in free electron density; the plasma frequency can be written for FCC metals as

$$\omega_p^2 = \frac{4e^2}{\varepsilon_0 m_{eff} a^3}, \tag{6}$$

where e is the electric charge and a is the deformed, or strained lattice constant; we note that $a_0 = 4.08\,\text{Å}$ is the undeformed lattice constant for gold. Clearly, any variation in the lattice constant a due to mechanical strain will impact the plasma frequency ω_p, which will result in either a blue or redshift of the optical spectra.

Furthermore, any strain-induced change in lattice constant a also impacts the Fermi velocity v_F in (3); this is because the Fermi energy can be written as

$$E_F = \frac{h^2}{2m}\left(\frac{3}{8\pi}\right)^{2/3} N^{2/3}, \tag{7}$$

where h is Planck's constant, m is the electron mass, and N is the electron density. Because the electron density N can be written as, for FCC metals

$$N = \frac{4}{a^3}, \tag{8}$$

and noting that the Fermi velocity can be written in terms of the Fermi energy

$$V_F = \sqrt{\frac{2E_F}{m}}, \tag{9}$$

it is clear from (9) that any change in the electron density N due to strain effects on the lattice constant a will change both the Fermi velocity V_F and the Fermi energy E_F.

However, as discussed by Lerme et al. (2001), imposed mechanical strain not only affects the dielectric function of the free, or conduction electrons, but also affects the dielectric function for the ionic core, or bound electrons. This can be written as

$$\varepsilon_{core}(\omega) \to \frac{\varepsilon_{core}(\omega)+2+2v(\varepsilon_{core}(\omega)-1)}{\varepsilon_{core}(\omega)+2-v(\varepsilon_{core}(\omega)-1)}, \tag{10}$$

where v captures the strain-induced change in lattice constant as

$$v = \left(\frac{a_0}{a}\right)^3. \tag{11}$$

We note that the correction to the dielectric function for the ionic core electrons in (10) is based upon classical theories, which neglect quantum effects such as electron spill out that lead to a blueshift in small metal nanostructures (diameter < 2 nm) with decreasing size. In other words, as discussed by Liebsch (1993), in quantum models due to the spillout effect, fewer electrons are inside the nanoparticle, and therefore fewer electrons are sensitive to the lattice contraction effects on $\varepsilon_{core}(\omega)$ in (10). However, in the present work, the nanoparticle diameters are all 10 nm or greater; therefore, such quantum-driven electron spillout effects can safely be neglected.

We wish to make other relevant comments with regards to how strain is assumed to impact the dielectric functions. First, we note that the functional forms we have used to incorporate strain effects, i.e. through (11) and (6), are specific to hydrostatic types of deformation. For hydrostatic and other generalized forms of deformation, the critical factor to account for is the change in the atomic unit cell volume that occurs due to the deformation (where the volume of the unit cell a^3 is seen in the denominator of (6) and (8)); it should be possible to do this by relating changes in unit cell volume to the generalized strain or deformation tensor. Second, we note that we have neglected variations in the electron effective mass that could occur either due to changes in nanosphere diameter or due to strain. We note that an extended discussion on this topic can be found in Lerme et al. (2001), where it is concluded that both strain effects and size effects are likely to impact the effective electron mass; however, the exact relationships appear to be currently unknown.

In summary, the final classical dielectric functions for gold are found by modifying the bulk dielectric functions of Johnson and Christy (1972) by accounting for the previously described effects from surface damping (Coronado and Schatz, 2003), lattice contraction effects on the free electron density (Cai et al., 2001), and lattice contraction effects on the ionic core (Lerme et al., 2001) by combining (5), (6) and (10).

3. Numerical methodology

To calculate the optical spectra of the spherical gold nanoparticles, we utilize Mie scattering theory (Mie, 1908). The advantage of Mie theory as compared to numerical methods to solve Maxwell's equations such as the finite difference time

domain (FDTD) (Yee, 1966) and discrete dipole approximation (DDA) (Purcell and Pennypacker, 1973) methods is that Mie theory provides analytic solutions to Maxwell's equations for a restricted number of geometries, most typically spheres.

Within Mie theory, expressions for the extinction, scattering and absorption efficiencies for spherical particles that are subject to a beam of linearly polarized incident light are written as

$$Q_{ext} = \frac{2}{x^2}\sum_{n=1}^{\infty}(2n+1)\mathrm{Re}(a_n+b_n) \tag{12}$$

and

$$Q_{sca} = \frac{2}{x^2}\sum_{n=1}^{\infty}(2n+1)\{|a_n|^2+|b_n|^2\}. \tag{13}$$

Because extinction is simply the sum of the absorption and scattering efficiencies, i.e. $Q_{ext} = Q_{abs} + Q_{sca}$, the absorption efficiency can be written as

$$Q_{abs} = \frac{2}{x^2}\sum_{n=1}^{\infty}(2n+1)\{\mathrm{Re}(a_n)-|a_n|^2+\mathrm{Re}(b_n)-|b_n|^2\}, \tag{14}$$

where a_n and b_n are

$$a_n = \frac{\psi_n'(mx)\psi_n(x)-m\psi_n(mx)\psi_n'(x)}{\psi_n'(mx)\zeta_n(x)-m\psi_n(mx)\zeta_n'(x)} \tag{15}$$

and

$$b_n = \frac{m\psi_n'(mx)\psi_n(x)-\psi_n(mx)\psi_n'(x)}{m\psi_n'(mx)\zeta_n(x)-\psi_n(mx)\zeta_n'(x)}, \tag{16}$$

where m is the refractive index of the sphere, $x = 2\pi(\varepsilon_m)^{0.5} r\lambda^{-1}$, r is the radius of the sphere, λ is the wavelength of the incident beam of light, ε_m is the dielectric function of the surrounding medium, and ψ and ζ are Riccati–Bessel functions (Jain et al., 2006).

We note that the strain effects on the dielectric functions that were described in the previous section enter Eqs. (12)–(14) in two ways. First, the refractive index m is defined as the square root of the dielectric function, i.e. $m = \sqrt{\varepsilon}$. Therefore, because the dielectric function we use is strain-corrected, all Mie parameters are impacted by the strain modified refractive index m. Second, the expression for x in Eqs. (12)–(14) is impacted by strain due to the corresponding expansion or contraction of the sphere radius r.

We note that cross sections for extinction (C_{ext}), scattering (C_{sca}) and absorption (C_{abs}) can be obtained by multiplying the results in (12)–(14) by the actual cross sectional area of the spherical particles projected on the plane which is perpendicular to the wave vector of incident light. We further note that the extinction cross section has the physical meaning of being the total area of the incident beam of light that is removed by the metal nanoparticle. Similarly, the scattering cross section represents the area of the incident beam of light that is redirected from its initial direction of propagation, while the absorption cross section represents the area of the incident beam of light that is removed by being absorbed by the nanoparticle (Grady et al., 2004). Efficiencies represent cross sections normalized by the cross sectional area of particle, which facilitate comparison between particles of different sizes; such comparisons will be made later in this work.

In the following numerical simulations, we calculate the absorption (Q_{abs}) and scattering (Q_{sca}) efficiencies using the BHMIE code of Bohren and Huffman (1983), while the local electric field enhancement (SERS) factors are found using the SPlaC code of Le Ru and Etchegoin (2009).

4. Numerical results and discussion

We performed Mie calculations on spherical gold nanoparticles with diameters of 10, 20, 40, 80 and 100 nm, where the surrounding medium was assumed to be air in all cases, i.e. $\varepsilon_m = 1$. For each nanoparticle size, we calculated the extinction, scattering and absorption spectra for strains between -5% (compressive) and 5% (tensile), with increments of 1% strain in between.

We first show in Fig. 1 the absorption and scattering spectra for a 100 nm diameter gold nanosphere as a function of tensile and compressive strain. There are specific trends that we wish to point out. First, we see that applied tensile strain leads to both blueshifts in the plasmon resonance wavelength, and an increase in both the absorption and scattering efficiencies as compared to the unstrained (bulk) value. To quantify, the blueshift of the absorption maximum at 5% tensile strain is nearly 40 nm, while the blueshift of the scattering maximum is about 28 nm; furthermore, the scattering efficiency is enhanced about 95% from 1.41 to 2.75, while the absorption efficiency is enhanced about 12%, from 2.61 to 2.92.

However, if compressive strain is applied, we observe both a redshift in the plasmon resonance wavelength and also a reduction in both the absorption and scattering efficiencies. To quantify, when 5% compressive strain is applied, the

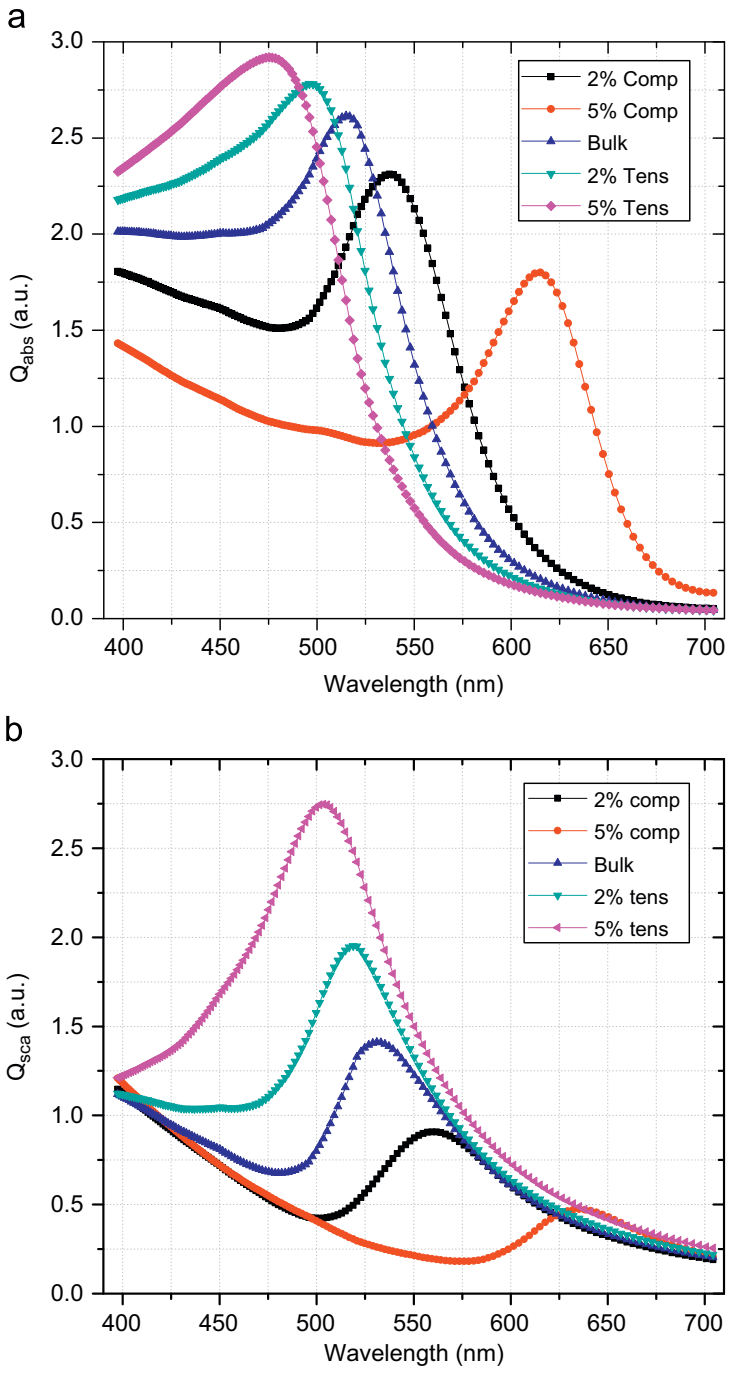

Fig. 1. Plots of (a) absorption (strain-induced Q_{abs} for 100 nm gold nanosphere) and (b) scattering (strain-induced Q_{sca} for 100 nm gold nanosphere) efficiencies for a 100 nm diameter gold nanoparticle as a function of strain.

redshifts of both spectra are over 100 nm, while the absorption efficiency is reduced by nearly 31% from 2.61 to 1.8, and the scattering efficiency is reduced by nearly 66% from 1.41 to 0.47.

The trends observed for the 100 nm diameter gold nanospheres are also found for the smaller diameter nanospheres. Specifically, tensile strains lead to blueshifts in the plasmon resonance wavelength, and increases in both the absorption and scattering efficiencies, while compressive strains lead to redshifts in the plasmon resonance wavelength, and reductions in the absorption and scattering efficiencies. The major difference for the smaller diameter nanospheres is the increasing importance of surface damping effects with decreasing nanosphere diameter; surface damping becomes important when the nanoparticle size becomes smaller than the electron mean free path (Coronado and Schatz, 2003), where the electron mean free path in gold is about 50 nm (Link and El-Sayed, 1999a). The effect of surface damping is to reduce the absorption and scattering efficiencies, where the reduction is more than one order of magnitude for the smallest (10 nm) diameter nanosphere that we have considered.

We note that for the nanosphere diameters we have considered, the plasmon resonance wavelength shift as well as the increase or decrease in efficiency is different for absorption as compared to scattering. The reason for this can be seen from

the analytic Mie theory solutions for absorption and scattering efficiency in Eqs. (13) and (14), which show different dependencies on the Mie coefficients a_n and b_n. The fact that the absorption and scattering of a single metal nanoparticle can be tuned at different incident wavelengths of light by utilizing mechanical strain opens up the possibility of multifunctional metal nanoparticles which can be used for both optical imaging (scattering) and photothermal cancer therapy (absorption), as in Gobin et al. (2007).

In analyzing these results, it is evident that while the plasmon resonance wavelength can be tuned and shifted using both tensile and compressive mechanical strain, the decrease in the absorption, scattering and extinction efficiencies that occurs due to compressive strain is somewhat undesirable for practical applications. This is because reducing the scattering and absorption efficiencies will directly lead to lower local heat generation due to absorption for photothermal cancer treatments, and lower resolution of the nanoparticles through light scattering for optical sensing and detection applications. In contrast, the enhancement of absorption and scattering efficiencies due to tensile strain along with the tunability of the plasmon resonance wavelength indicates that tensile mechanical strain is likely to be more beneficial in tailoring the optical properties of spherical metal nanoparticles.

A pertinent question that needs to be addressed before continuing with further analysis is whether inelastic crystalline deformation such as dislocations, which would result in the nanoparticle as a result of the large tensile and compressive strains we have imposed, would significantly impact the strain-induced optical properties that we report in the present work. Preliminary evidence in the literature has suggested that such crystalline defects would not impact the far field optical properties (extinction, absorption, scattering) that we have calculated in the present work. Justification for this comes from previous experimental results (Hao et al., 2004) and theoretical calculations (Hao et al., 2004; Oubre and Nordlander, 2004). Both of these works investigated the effects of surface defects and voids, dimples and colloids on the optical properties of metal nanoshells. In doing so, both found that the far field optical properties (absorption, scattering, extinction) are fairly insensitive to such defects. However, both works found that the near field properties were significantly different, i.e. the local electric fields near such surface defects were enhanced by factors of almost 10 (Hao et al., 2004).

However, we note that the works discussed above as well as the present work have neglected certain aspects of defect/dielectric function interactions that may be significant. For example, it is likely that dislocations near the surfaces of materials will most strongly impact the plasma frequency ω_p in (6) by changing the electron density due to the slip of crystalline planes of atoms. Similarly, dislocations generated within the nanoparticle bulk would most likely impact the core, or bound electron dielectric function in (10). Furthermore, the separation between surface and bulk defects and their effects on both the free and core electron dielectric functions will become blurred as the size of the nanoparticles decreases, leading to increased interactions between surface and bulk atoms. Finally, charge screening effects are likely to be different within the bulk as compared to at the surfaces of the nanoparticles, which would also impact both the free and core electron dielectric functions; it is currently unclear whether these effects could be captured within the classical framework utilized in the present work, or whether quantum modifications would be required. In the present work, we thus adopt the approximation that neither the near field (SERS) nor far field optical properties are greatly impacted by the deformation of the metal nanoparticles.

At this point, we continue forward onto an extensive analysis of some pertinent issues related to strain effects on the optical properties of gold nanoparticles, including the impact on the absorption and scattering efficiencies, the red and blueshifts of the plasmon resonance wavelength, the local electric field enhancement, which has implications for SERS, the importance of the dielectric functions, and an analysis of size effects and size-normalized absorption and scattering cross sections. These issues are treated individually below.

4.1. *Influence of dielectric functions on the far field optical efficiencies and the wavelength shifts of the plasmon resonance*

We now investigate the origins of the strong strain-dependence of the optical properties of gold nanoparticles as well as the origins of the red and blueshift of the plasmon resonance wavelength due to applied strain, and the enhancement and reduction in far field optical efficiencies due to applied strain. Because of its dominant effect in the following discussion, we stress that it is the interband transitions of the core (bound) electrons from the valence band to the Fermi surface which dominates the plasmon resonance of gold in the visible spectrum, and that the interband transition occurs around $\lambda_{IB}=470$ nm for gold (Wang et al., 2005; Etchegoin et al., 2006; Lee and El-Sayed, 2005, 2006).

We therefore plot in Fig. 2 the ionic core contribution to the real and imaginary parts of the dielectric function for a 10 nm diameter gold nanosphere subject to both tensile and compressive strain. The figure clearly shows that the core dielectric function ε_{core} is substantially impacted by strain, or more specifically compressive strain. In particular, Fig. 2 shows that interband transitions due to the core, or bound electrons in gold occur around $\lambda_{IB}=470$ nm in unstrained bulk gold. Furthermore, we have found that for the gold nanoparticles of varying diameter that we have studied, that the variations in ε_{core} show very little size-dependence. In addition, our numerical results show that the strain-induced variation of the Drude dielectric term ε_{free} is negligible in comparison to the strain-induced variation in ε_{core}. Therefore, for incident wavelengths of light that are comparable to the interband transition wavelength $\lambda_{IB}=470$ nm, the interband transitions, and therefore the effects of the core electrons dominate the dielectric function ε; we will demonstrate that it is

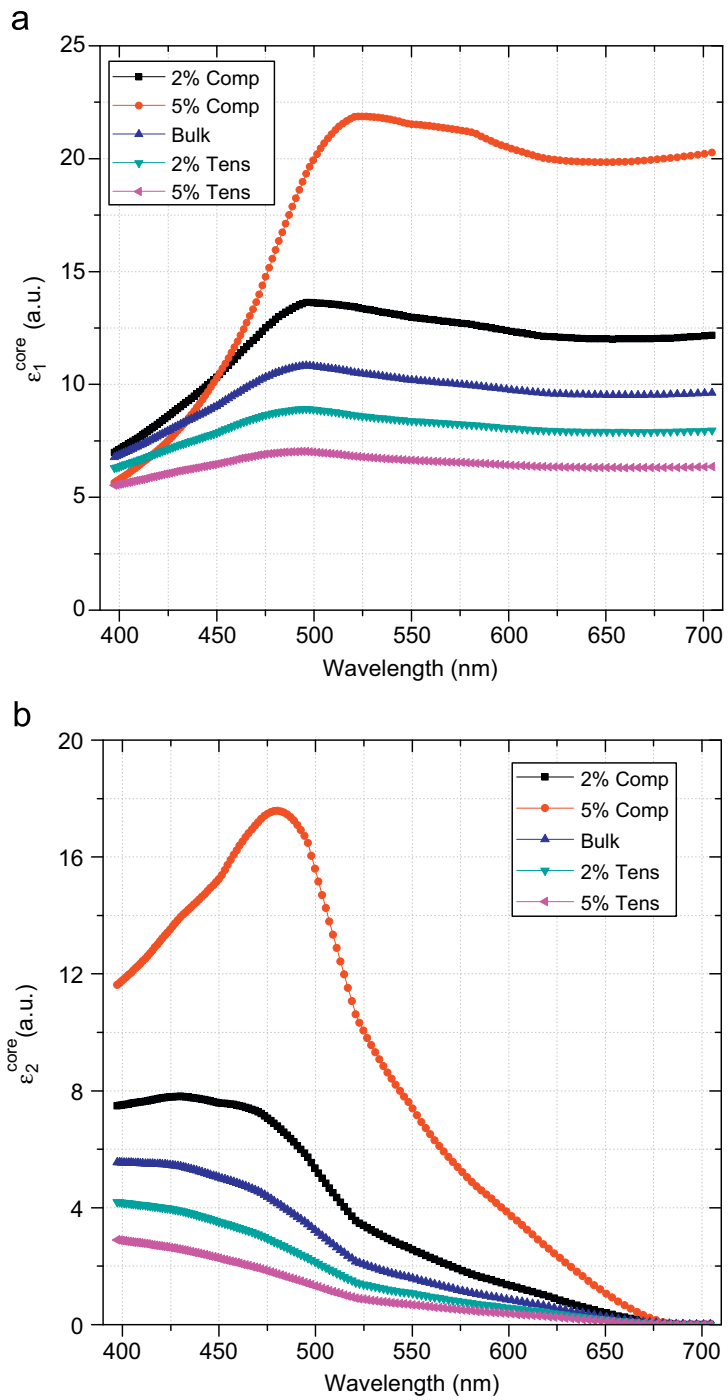

Fig. 2. Real (a) ε_1^{core} (ε_1^{core} Contribution of 10 nm Gold Nanosphere) and imaginary (b) ε_2^{core} (ε_2^{core} Contribution of 10 nm Gold Nanosphere) contributions to the dielectric function of a 10 nm diameter gold nanosphere as a function of strain.

the core contribution to the dielectric function that explains the effects of compressive strain on the optical properties of gold nanoparticles.

Fig. 2 gives other valuable information regarding the effects of strain on the far field optical properties of gold nanoparticles. In particular, it demonstrates that compressive strain increases ε_{core} and tensile strain damps ε_{core}, while the increase in ε_{core} due to compression exceeds the decrease in ε_{core} that occurs due to tension. These strain-induced shifts in the dielectric properties can be directly related to the observed changes in far field optical efficiencies as well as the wavelength shifts in the plasmon resonance, as we now discuss.

For example, the imaginary part of the core dielectric function ε_2^{core} shows a significant enhancement due to compressive strain in Fig. 2b; because an increase in the imaginary part of the dielectric function, which represents an enhancement in the active damping mechanisms, is known to strongly reduce the magnitude of the far field optical efficiency (Coronado and Schatz, 2003; Lee and El-Sayed, 2006), this explains the reduced scattering and absorption efficiencies that was observed in Fig. 1 due to compressive strain.

We also address the origins underlying the blueshift that we have reported with increasing tensile strain, and the redshift we have found that occurs with increasing compressive strain in Fig. 1. In particular, it is known that ε_{core} causes the dielectric screening of the surface charge, which reduces the restoring force that results from the electrical field that is experienced by the free or conduction electrons in the Drude model; this has the effect of reducing the overall plasmon resonance frequency, which then results in a redshift of the total plasmon resonance wavelength with increasing ε_{core} (Grady et al., 2004). In contrast, decreasing ε_{core} would result in a blueshift of the total plasmon resonance wavelength.

As seen in Fig. 2, ε_1^{core} increases from about 11 to 22 at 5% compressive strain, while ε_1^{core} decreases from about 11 to 7 at 5% tensile strain. Because the increase in ε_1^{core} due to compressive strain exceeds the decrease in ε_1^{core} due to tensile strain, we would expect a larger redshift due to compression than the blueshift due to tension for the 10 nm diameter gold nanoparticles. In fact, as previously discussed, this is exactly what is observed; the redshift due to 5% compression exceeds 100 nm for both absorption and scattering, while the blueshift due to 5% tension is about 70 nm for scattering and about 92 nm for absorption.

4.2. Size effects on the strain-induced changes of both the wavelength shift of the plasmon resonance and the far field optical efficiencies

We next study the effects of nanoparticle size on the strain-induced changes in both the wavelength shift of the plasmon resonance and also the efficiencies of the far field optical properties. We first plot the wavelength shift of the maxima of the absorption and scattering spectra due to strain as a function of nanoparticle size in Fig. 3. There emerge three interesting trends that can be observed in Fig. 3 which we will analyze further. First, the compressive-strain-induced resonance wavelength shift appears to be nearly independent of the nanosphere diameter. Second, the compressive-strain-induced redshifts are larger than the tensile-strain-induced blueshifts. Third, the tensile-strain-induced blueshifts for the large diameter nanospheres (80 and 100 nm) are significantly smaller than the tensile-strain-induced blueshifts for the smaller diameter nanospheres (10, 20 and 40 nm).

First, the reason that the compressive-strain-induced resonance wavelength shift is essentially size-independent can be gleaned from studying (Fig. 1) as well as the dielectric functions in Fig. 2(a). Fig. 1 demonstrates that the compressive-strain-induced resonance wavelengths are greater than the bulk, unstrained resonance wavelength of about 520 nm. Because the change in slope $d\varepsilon_1^{core}/d\lambda \approx 0$ for all nanosphere sizes and for wavelengths greater than about 520 nm, and because the real part of the dielectric function and its associated derivatives play the key role in determining the plasmon resonance wavelength (Lee and El-Sayed, 2005, 2006), we have explained why the compressive-strain-induced redshifts for gold nanospheres of different diameters are nearly size-independent.

Next, we address the reasons underlying the fact that the compressive-strain-induced redshifts are larger than the tensile-strain-induced blueshifts. This can be understood by noting that the compressive-strain-induced variation in ε_1 exceeds the change in ε_1 due to tensile strain. For example, at an incident wavelength of 525 nm, 5% compressive strain increases ε_1^{core} to 21.9 relative to the unstrained value of 10.48, while 5% tensile strain decreases the value of ε_1^{core} to 6.8.

Finally, we address the third trend that the tensile-strain-induced blueshifts for the large diameter nanospheres (80 and 100 nm) are significantly smaller than the tensile-strain-induced blueshifts for the smaller diameter nanospheres (10, 20 and 40 nm). The reason for this is likely due to the effects of both dynamic depolarization and retardation (Kelly et al., 2003; Myroshnychenko et al., 2008) on the plasmon resonance wavelengths of larger metal nanoparticles (Wokaun et al., 1982; Meier and Wokaun, 1983; Noguez, 2005), both of which occur due to the breakdown of the quasistatic approximation for larger nanoparticle diameters, i.e. the nanoparticle no longer interacts homogeneously with the incident electromagnetic wave.

We also show in Fig. 4 the percent change in the absorption and scattering efficiencies as compared to the bulk, unstrained gold nanoparticles. As seen in Fig. 4 b, there is a substantial gain in scattering efficiency due to tensile strain, which far exceeds the reduction in scattering efficiency due to compressive strain. Again, this is due to the fact that the enhancement in dielectric function damping due to compression, as seen in Fig. 2b, far exceeds the reduction in damping due to tension. In particular, the scattering efficiency drops nearly 70% at 5% compressive strain; however, it increases 126% at 5% tensile strain.

Similar trends are observed for the strain and size-dependent absorption efficiencies in Fig. 4a. As can be observed, the increase in the absorption and scattering efficiencies due to tensile strain is again significantly larger than the decrease in the efficiencies induced by compressive strain. Specifically, the absorption efficiency drops by 37% compared to an unstrained nanoparticle at 5% compressive strain while an increase in efficiency of nearly 57% is observed at 5% tensile strain. We also note the decrease in tensile-strain-induced efficiency gain for larger nanoparticles, which may also be attributed to dynamic depolarization effects coupled with the enhanced absorption due to the fact that the corresponding resonance wavelengths are somewhat far from the interband transition edge of gold at 470 nm (Wang et al., 2005; Etchegoin et al., 2006).

These effects, coupled with the fact that scattering tends to dominate the extinction spectra of larger metal nanoparticles, explains the loss in tensile strain-induced gains in absorption efficiency for larger nanoparticle sizes observed in Fig. 4a.

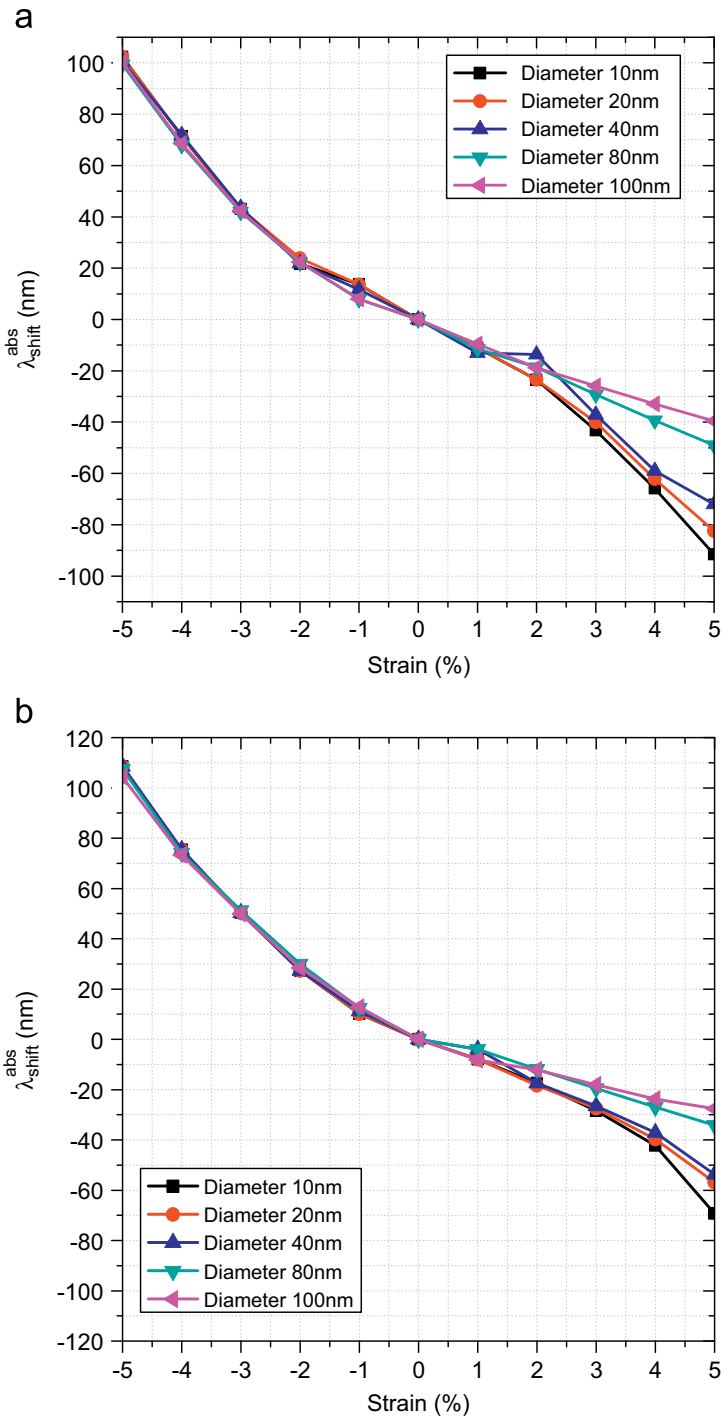

Fig. 3. Strain-induced shift in plasmon resonance wavelength for (a) absorption (resonance wavelength shift of Q_{abs}) and (b) scattering (resonance wavelength shift of Q_{sca})of gold nanoparticles.

4.3. *Strain effects on the local electric field and SERS*

We now discuss how mechanical strain impacts the local E-field, and thus the SERS enhancement of spherical gold nanoparticles. Before presenting our analysis, we define the local E-field intensity (Le Ru and Etchegoin, 2009) and surface-enhanced Raman scattering enhancement factor (SERS-EF) (Garcia-Vidal and Pendry, 1996) as

$$M_{loc}(\mathbf{r}_m,\omega)=\left|\frac{\mathbf{E}(\mathbf{r}_m,\omega)}{E_{inc}(\omega)}\right|^2 \tag{17}$$

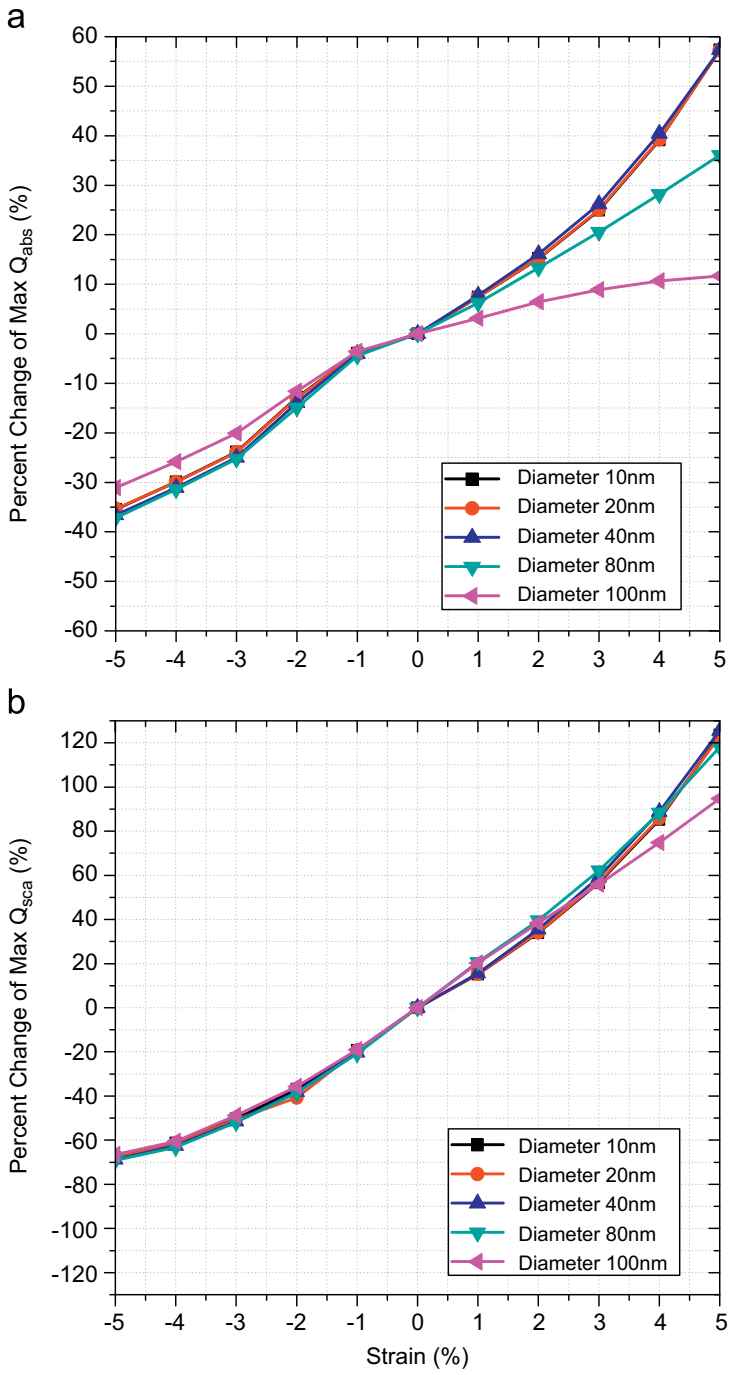

Fig. 4. Strain-induced percent change in (a) absorption (strain-induced change of max Q_{abs}) and (b) scattering (strain-induced change of max Q_{sca}) efficiencies of gold nanoparticles.

and

$$\rho(\mathbf{r}_m,\omega)=\left|\frac{\mathbf{E}(\mathbf{r}_m,\omega)}{E_{inc}(\omega)}\right|^4, \tag{18}$$

where M_{loc} is the local E-field intensity, ρ is the SERS enhancement factor, $E_{inc}(\omega)$ is the electric field due to the incident plane wave, and $\mathbf{E}(\mathbf{r}_m,\omega)$ is the total electric field at position $\mathbf{r}_m$.

We illustrate our findings by showing in Fig. 5 the M_{loc} value as a function of distance away from the surface of the 100 nm diameter gold nanosphere for three cases: no strain (bulk), 5% compressive strain, and 5% tensile strain. First, Fig. 5 demonstrates that the largest enhancement of the E-field occurs just outside the surface of the gold nanoparticle, as is expected. Second, we note that 5% tensile strain increases the M_{loc} value nearly 28% to 40.2 as compared to the bulk, unstrained M_{loc} value of 31.5. In contrast, 5% compressive strain reduces the maximum M_{loc} value nearly 16% from 31.5 to 26.5.

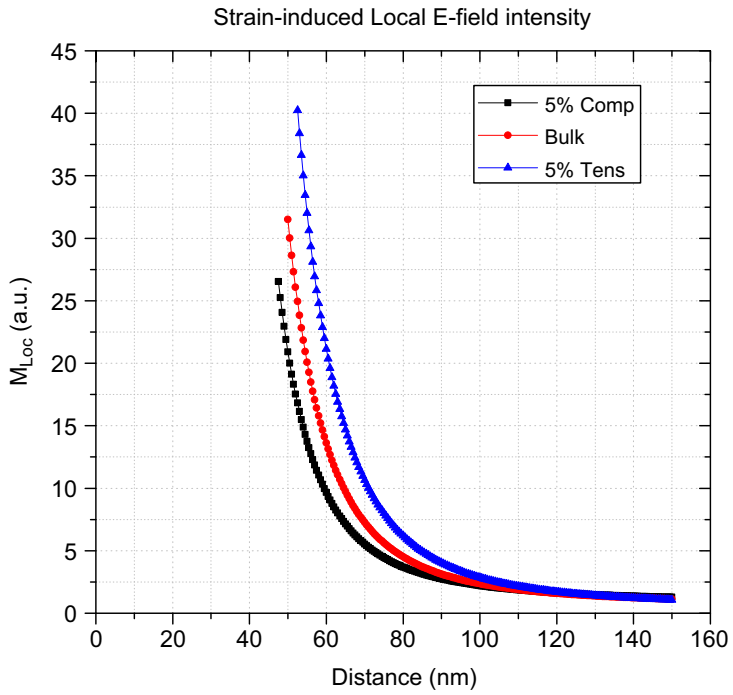

Fig. 5. Strain-induced local electric field intensity M_{loc} along the polarization axis of a 100 nm diameter gold nanosphere. The M_{loc} values are plotted starting at the surface of the nanosphere (radius = 50 nm) moving away from the nanosphere interior.

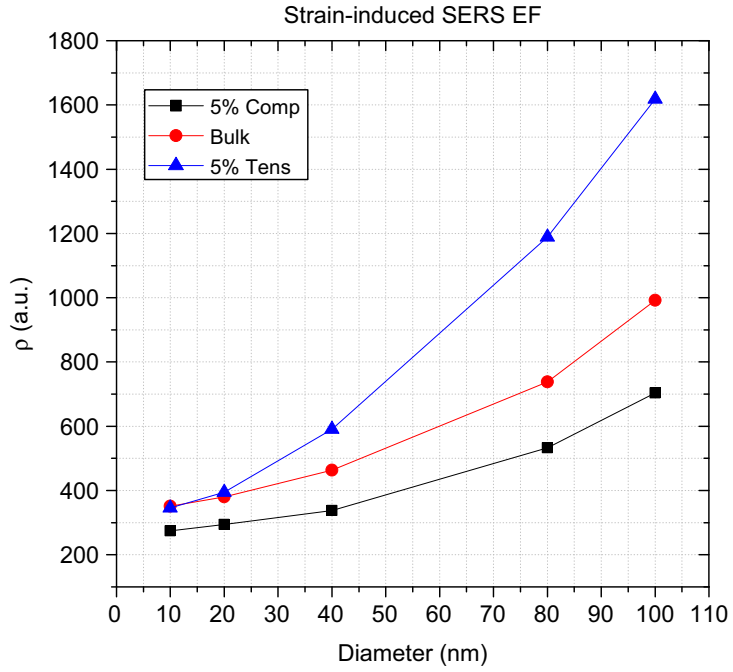

Fig. 6. Strain-induced SERS enhancement factors (SERS-EF) ρ for 10, 20, 40, 80 and 100 nm diameter gold nanospheres.

We also show in Fig. 6 the maximum SERS enhancement factor (ρ) as a function of nanoparticle size and strain. We first notice that as the gold nanoparticle diameter increases, the SERS enhancement factor also increases; this is due to the fact that as the nanoparticle diameter increases, scattering becomes the dominant contribution to the nanoparticle extinction spectra (Lee and El-Sayed, 2005). We also note that compressive strain reduces the ρ values. Specifically, the ρ increases are 0, 4%, 28%, 61% and 63% for the 10, 20, 40, 80 and 100 nm diameter particles due to 5% tensile strain, while the ρ decreases are 22%, 23%, 27%, 28% and 29% due to 5% compressive strain for the same size nanoparticles.

An interesting trend that is observed in Fig. 6 is that the tensile strain-induced gain of ρ is nearly proportional to the nanosphere diameter. The reason for this trend is linked to the difference between the tensile strain-induced ε_2 and the bulk value of ε_2 for the plasmon resonance wavelength at the different nanosphere diameters we have considered. We plot

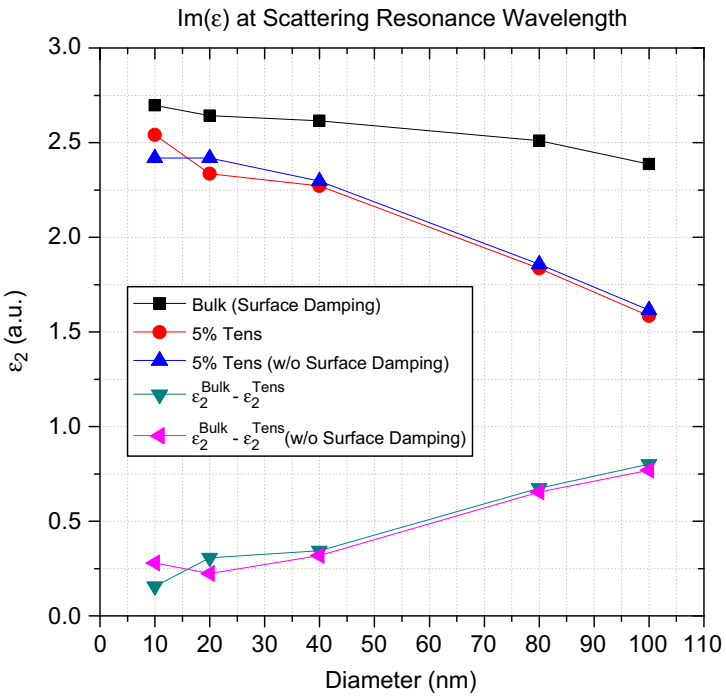

Fig. 7. Comparison of bulk and tensile strain-induced ε_2 for 10, 20, 40, 80 and 100 nm diameter gold nanospheres.

these ε_2 in Fig. 7, which demonstrates that 5% tensile strain reduces ε_2 and also that the difference between the tensile strain-induced ε_2 and the bulk ε_2 increases as the nanosphere diameter increases. More importantly, we also plot the imaginary part of the dielectric function both with and without the surface damping effects of Coronado and Schatz (2003). As can be seen, the surface damping effects are only important for the 10 and 20 nm diameter gold nanospheres, where for the 10 nm nanosphere it is observed that surface damping eliminates much of the reduction in ε_2 that is gained through the application of tensile strain. The diameters at which the surface damping effects correlate well with the established value for the electron mean free path in gold, which is typically stated to be around 50 nm (Link and El-Sayed, 1999a).

According to our previous discussion, larger values of the imaginary part of ε_2 lead to a weaker plasmon resonance, and also a reduced local electric field magnitude. In this respect, the increase in the $\varepsilon_2^{Bulk}-\varepsilon_2^{Tens}$ term in Fig. 7 with increasing nanosphere diameter explains why for very small diameters in Fig. 6, the tensile strain-induced SERS enhancement factor (ρ) is small, and why the gain in ρ increases with increasing nanosphere diameter.

We have thus demonstrated that tensile mechanical strain can be a useful mechanism for enhancing the SERS effect in gold nanoparticles, and particularly for larger (diameter greater than 20 nm) gold nanoparticles, which may be relevant in a variety of applications (Oldenburg et al., 1998; Sun and Xia, 2003; Barnes et al., 2003; Anker et al., 2008). We note that these enhancements due to tensile strain, which approach a factor of 2, are similar to ρ enhancements of 2–4 that have been found due to voids and pinholes on the surfaces of metal nanoshells (Hao et al., 2004; Oubre and Nordlander, 2004), and which have been found to be useful for SERS applications.

4.4. Size-normalized absorption and scattering cross sections

Finally, we discuss the size-normalized absorption and scattering cross sections of the gold nanoparticles. Following Jain et al. (2006), we note that the absolute magnitude of the absorption and scattering cross-sections may not be a reliable gauge of the optical properties of nanoparticles being utilized in biomedical engineering applications, where it is possible that smaller particles can be bounded in a given volume in greater numbers when compared to particles of larger sizes. In this case, a more reasonable property for comparison is the size-normalized cross section C/V, where C denotes the cross section of interest (absorption or scattering) and V the volume of the nanoparticle. If expressed in units of μm^{-1}, we can obtain the per micron absorption coefficient (ACPM) and scattering coefficient (SCPM) for the gold nanoparticles.

We should note two differences between the present results and those given in Jain et al. (2006). First, we have calculated the ACPM and SCPM where the surrounding medium is air, and not water. Because the dielectric constant of air is smaller than that of water, our ACPM and SCPM values are smaller than those given by Jain et al. (2006) for the same nanoparticle diameter. Second, we have calculated the ACPM and SCPM at the wavelengths where the absorption and scattering efficiencies have their maximum value; this differs slightly from the procedure of Jain et al. (2006), where all values were computed at the maximum extinction wavelength. This is necessary because strain causes the absorption and scattering maxima for the larger diameter nanoparticles to differ from the extinction maximum wavelength; smaller

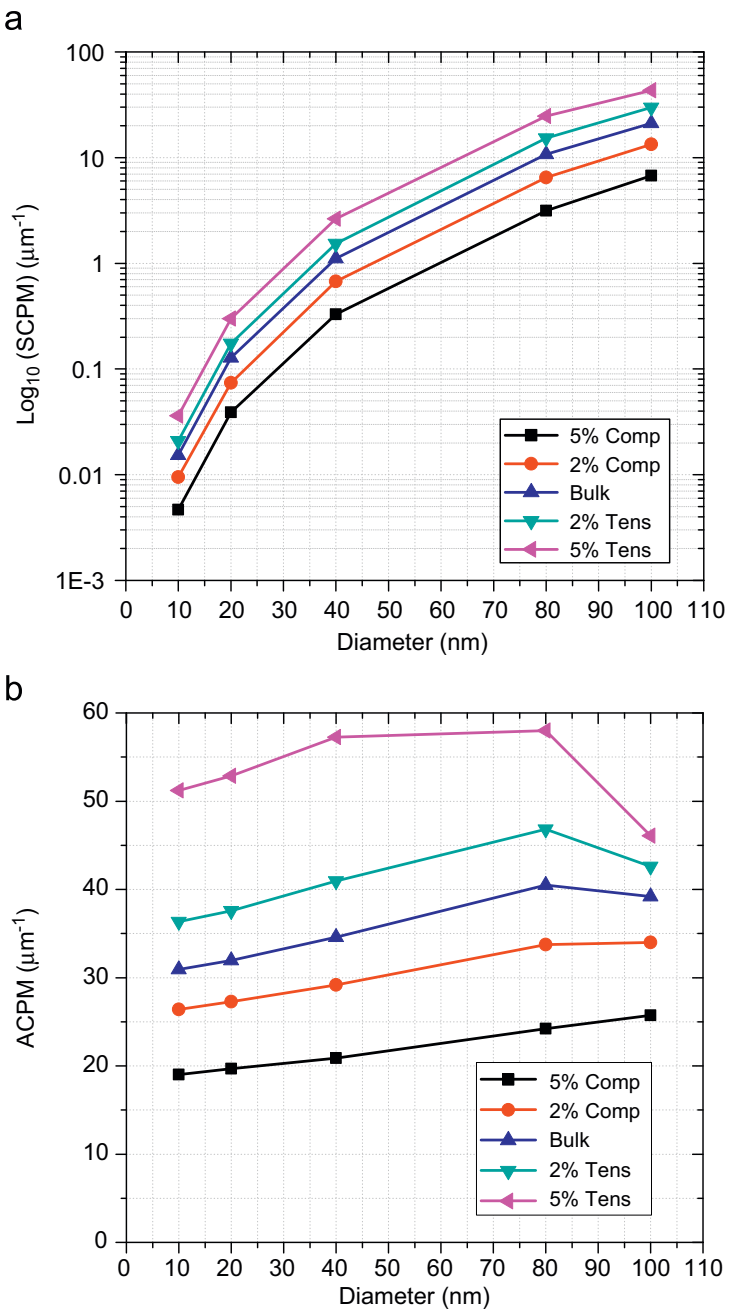

Fig. 8. (a) Scattering coefficients per micron (SCPM) (strain induced change of max Q_{abs}) and (b) absorption coefficients per micron (ACPM) (strain induced change of max Q_{sca}) for gold nanoparticles of various diameters.

nanoparticles, due to the quasistatic approximation, have absorption and scattering maximum wavelengths that coincide with the extinction maximum wavelength.

From Fig. 8a, we find that the SCPM is strongly dependent on the size of gold nanoparticles, where larger nanoparticles are seen to be preferable for applications where a high scattering efficiency is necessary, which is in agreement with previous studies (Jain et al., 2006). However, Fig. 8a also demonstrates that for the entire range of nanoparticle sizes, the size-normalized scattering cross section can be essentially doubled through application of 5% tensile strain, which may be valuable for applications where large scattering cross sections are required.

In contrast, Fig. 8b demonstrates that the size-normalized absorption cross sections are found to be relatively size-independent, where the ACPM for 5% tensile strain is found to hover around 50 μm^{-1} for the entire range of nanoparticle diameters we have considered. Furthermore, the application of 5% tensile strain is found to enhance the ACPM by about 50% across the range of nanoparticle diameters we have considered, which indicates the robust nature of tensile strain in enhancing both the absorption and scattering cross sections for practical applications. Specifically, 5% tensile strain is found to increase the ACPM by 65.6%, 65.5%, 65.6%, 43% and 17.6% for the 10, 20, 40, 80 and 100 nm diameter gold nanoparticles, respectively, where the decrease in ACPM for the 80 and 100 nm diameter nanoparticles is due to the

dynamic depolarization effects resulting from the breakdown of the quasistatic approximation, as was previously discussed in Section 4.2.

5. Conclusions

In conclusion, we have demonstrated, using classical Mie theory with size and strain-corrected dielectric functions, that mechanical strain has a significant effect on the optical properties of gold nanospheres. In particular, we have found that tensile mechanical strain leads to substantial enhancements in the absorption and scattering maxima of the nanoparticles, in addition to a significant blueshift in the plasmon resonance wavelength. Furthermore, tensile strain was shown to improve the SERS ($|E|^4$) enhancement by nearly a factor of 2, while also enhancing the volume normalized absorption and scattering cross sections for the nanoparticles across a range technologically relevant nanoparticle diameters.

In contrast, compressive mechanical strain was found to have the opposite effect as tensile strain on the optical properties, causing a redshift in the plasmon resonance wavelength, a reduction in absorption and scattering maxima, and a reduction in the both the SERS enhancement as well as the volume normalized absorption and scattering cross sections. Furthermore, the difference between tensile and compressive strain effects was shown to be related to their effects on the core dielectric function, due to the fact that the interband transition wavelength in gold is nearly coincident with the plasmon resonance wavelength.

We close with a few other relevant comments. First, biomedical applications typically require nanoparticles to absorb or scatter strongly in the near infrared (NIR) region, i.e. 650–900 nm, such that light can penetrate through tissue and not be absorbed by hemoglobin or other chromophores (Weissleder, 2001). The plasmon resonance wavelengths of the gold nanoparticles are typically smaller than this, i.e. in the $\lambda = 520$ nm range, thus limiting their applicability for biomedical applications. Therefore, a more relevant approach that researchers have taken recently is to utilize gold nanorods and nanowires instead of nanoparticles, as the elongated geometry causes a redshift in the plasmon resonance wavelength into the NIR region. Our future work will then analyze how mechanical strain impacts the optical properties of nanostructures with different geometries such as nanorods and nanowires, which in addition to having plasmon resonance wavelengths in the NIR, have also been shown to be more efficient absorbers and scatters, particularly at NIR wavelengths (Jain et al., 2006).

Acknowledgments

H.S.P. and X.-H.Q. both gratefully acknowledge NSF Grant number CMMI-0750395 in support of this research as well as the insightful comments of the reviewers.

References

Alizadeh, A., Sharma, P., Ganti, S., LeBoeuf, S.F., Tsakalakos, L., 2004. Templated wide band-gap nanostructures. Journal of Applied Physics 95 (12), 8199–8206.
Anker, J.N., Hall, W.P., Lyandres, O., Shah, N.C., Zhao, J., Duyne, R.P.V., 2008. Biosensing with plasmonic nanosensors. Nature Materials 7, 442–453.
Audoit, G., Mhuircheartaigh, E.N., Lipson, S.M., Morris, M.A., Blau, W.J., Holmes, J.D., 2005. Strain induced photoluminescence from silicon and germanium nanowire arrays. Journal of Materials Chemistry 15, 4809–4815.
Barnes, W.L., Dereux, A., Ebbeson, T.W., 2003. Surface plasmon subwavelength optics. Nature 424, 824–830.
Bohren, C.F., Huffman, D.R., 1983. Absorption and Scattering of Light by Small Particles. Wiley-Interscience, New York.
Brongersma, M.L., Hartman, J.W., Atwater, H.A., 2000. Surface plasmon subwavelength optics. Physical Review B 62 (24), R16356–R16359.
Bryant, G.W., de Abajo, F.J.G., Aizpurua, J., 2008. Mapping the plasmon resonances of metallic nanoantennas. Nano Letters 8 (2), 631–636.
Cai, W., Hofmeister, H., Dubiel, M., 2001. Importance of lattice contraction in surface plasmon resonance shift for free and embedded silver particles. European Physical Journal D 13, 245–253.
Cammarata, R.C., 1994. Surface and interface stress effects in thin films. Progress in Surface Science 46 (1), 1–38.
Coronado, E.A., Schatz, G.C., 2003. Surface plasmon broadening for arbitrary shape nanoparticles: a geometrical probability approach. Journal of Chemical Physics 119 (7), 3926–3934.
Dalacu, D., Martinu, L., 2001. Optical properties of discontinuous gold films: finite-size effects. Journal of the Optical Society of America B 18 (1), 85–92.
El-Sayed, I.H., Huang, X., El-Sayed, M.A., 2005. Surface plasmon resonance scattering and absorption of anti-EGFR antibody conjugated gold nanoparticles in cancer diagnostics: applications in oral cancer. Nano Letters 5 (5), 829–834.
Etchegoin, P.G., Ru, E.C.L., Meyer, M., 2006. An analytic model for the optical properties of gold. The Journal of Chemical Physics 125 (16), 164705.
Fedrigo, S., Harbich, W., Buttet, J., 1993. Collective dipole oscillations in small silver clusters embedded in rare-gas matrices. Physical Review B 47 (16), 10706–10715.
Felidj, N., Aubard, J., Levi, G., 1999. Discrete dipole approximation for ultraviolet-visible extinction spectra simulation of silver and gold colloids. Journal of Chemical Physics 111 (3), 1195–1208.
Garcia-Vidal, F.J., Pendry, J.B., 1996. Collective theory for surface enhanced Raman scattering. Physical Review Letters 77 (6), 1163–1166.
Gobin, A.M., Lee, M.H., Halas, N.J., James, W.D., Drezek, R.A., West, J.L., 2007. Near-infrared resonant nanoshells for combined optical imaging and photothermal cancer therapy. Nano Letters 7 (7), 1929–1934.
Grady, N.K., Halas, N.J., Nordlander, P., 2004. Influence of dielectric function properties on the optical response of plasmon resonant metallic nanoparticles. Chemical Physics Letters 399, 167–171.
Hao, E., Li, S., Bailey, R.C., Zou, S., Schatz, G.C., Hupp, J.T., 2004. Optical properties of metal nanoshells. Journal of Physical Chemistry B 108, 1224–1229.
Hao, E., Schatz, G.C., 2004. Electromagnetic fields around silver nanoparticles and dimers. Journal of Chemical Physics 120 (1), 357–366.
Heyd, R., Charlier, A., McRae, E., 1997. Uniaxial-stress effects on the electronic properties of carbon nanotubes. Physical Review B 55 (11), 6820–6824.
Hirsch, L.R., Gobin, A.M., Lowery, A.R., Tam, F., Drezek, R.A., Halas, N.J., West, J.L., 2006. Metal nanoshells. Annals of Biomedical Engineering 34 (1), 15–22.

Hirsch, L.R., Stafford, R.J., Bankson, J.A., Sershen, S.R., Rivera, B., Price, R.E., Hazle, J.D., Halas, N.J., West, J.L., 2003. Nanoshell-mediated near-infrared thermal therapy of tumors under magnetic resonance guidance. Proceedings of the National Academy of Science 100 (23), 13549–13554.
Hovel, H., Fritz, S., Hilger, A., Kreibig, U., Vollmer, M., 1993. Width of cluster plasmon resonances: bulk dielectric functions and chemical interface damping. Physical Review B 48 (24), 18178–18188.
Huang, X., El-Sayed, I.H., Qian, W., El-Sayed, M.A., 2006. Cancer cell imaging and photothermal therapy in the near-infrared region by using gold nanorods. Journal of the American Chemical Society 128 (6), 2115–2120.
Jain, P.K., Lee, K.S., El-Sayed, I.H., El-Sayed, M.A., 2006. Calculated absorption and scattering properties of gold nanoparticles of different size, shape, and composition: applications in biological imaging and biomedicine. Journal of Physical Chemistry B 110, 7238–7248.
Jiang, H., Singh, J., 1997. Strain distribution and electronic spectra of InAs/GaAs self-assembled dots: an eight-band study. Physical Review B 56 (8), 4696–4701.
Johnson, H.T., Freund, L.B., Akyuz, C.D., Zaslavsky, A., 1998. Finite element analysis of strain effects on electronic and transport properties in quantum dots and wires. Journal of Applied Physics 84 (7), 3714–3725.
Johnson, P.B., Christy, R.W., 1972. Optical constants of the noble metals. Physical Review B 6 (12), 4370–4379.
Kelly, K.L., Coronado, E., Zhao, L.L., Schatz, G.C., 2003. The optical properties of metal nanoparticles: the influence of size, shape, and dielectric environment. Journal of Physical Chemistry B 107, 668–677.
Kittel, C., McEuen, P., 2004. Introduction To Solid State Physics. Wiley, New York.
Kneipp, K., Moskovits, M., Kneipp, H.E., 2006. Surface-Enhanced Raman Scattering. Springer, Berlin.
Kreibig, U., Genzel, L., 1985. Optical absorption of small metallic particles. Surface Science 156, 678–700.
Kresin, V.V., 1995. Collective resonances in silver clusters: role of d electrons and the polarization-free surface layer. Physical Review B 51 (3), 1844–1849.
Le Ru, E.C., Etchegoin, P.G., 2009. Principles of Surface-Enhanced Raman Spectroscopy and related plasmonic effects. Elsevier, Amsterdam.
Lee, K.-S., El-Sayed, M.A., 2005. Dependence of the enhanced optical scattering efficiency relative to that of absorption for gold metal nanorods on aspect ratio, size, end-cap shape, and medium refractive index. Journal of Physical Chemistry B 109, 20331–20338.
Lee, K.-S., El-Sayed, M.A., 2006. Gold and silver nanoparticles in sensing and imaging: sensitivity of plasmon response to size, shape, and metal composition. Journal of Physical Chemistry B 110, 19220–19225.
Lerme, J., Pellarin, M., Cottancin, E., Gaudry, M., Broyer, M., Fatti, N.D., Vallee, F., Voisin, C., 2001. Influence of lattice contraction on the optical properties and the electron dynamics in silver clusters. European Physical Journal D 17, 213–220.
Liebsch, A., 1993. Surface-plasmon dispersion and size dependence of Mie resonance: silver versus simple metals. Physical Review B 48 (15), 11317–11328.
Link, S., El-Sayed, M.A., 1999a. Size and temperature dependence of the plasmon absorption of colloidal gold nanoparticles. Journal of Physical Chemistry B 103, 4212–4217.
Link, S., El-Sayed, M.A., 1999b. Spectral properties and relaxation dynamics of surface plasmon electronic oscillations in gold and silver nanodots and nanorods. Journal of Physical Chemistry B 103, 8410–8426.
Liu, B., Jiang, H., Johnson, H.T., Huang, Y., 2004. The influence of mechanical deformation on the electrical properties of single wall carbon nanotubes. Journal of the Mechanics and Physics of Solids 52, 1–26.
Lyons, D.M., Ryan, K.M., Morris, M.A., Holmes, J.D., 2002. Tailoring the optical properties of silicon nanowire arrays through strain. Nano Letters 2 (8), 811–816.
Maier, S.A., Brongersma, M.L., Kik, P.G., Meltzer, S., Requicha, A.A.G., Atwater, H.A., 2001. Plasmonics—a route to nanoscale optical devices. Advanced Materials 13 (19), 1501–1505.
Malinsky, M.D., Kelly, K.L., Schatz, G.C., Duyne, R.P.V., 2001. Chain length dependence and sensing capabilities of the localized surface plasmon resonance of silver nanoparticles chemically modified with alkanethiol self-assembled monolayers. Journal of the American Chemical Society 123, 1471–1482.
Meier, M., Wokaun, A., 1983. Enhanced fields on large metal particles: dynamic depolarization. Optics Letters 8 (11), 581–583.
Mie, G., 1908. Contributions to the optics of the turbid media, particularly of colloidal metal solutions. Royal Aircraft Establishment.
Mock, J.J., Oldenburg, S.J., Smith, D.R., Schultz, D.A., Schultz, S., 2002. Composite plasmon resonant nanowires. Nano Letters 2 (5), 465–469.
Murphy, C.J., Jana, N.R., 2002. Controlling the aspect ratio of inorganic nanorods and nanowires. Acta Materialia 14 (1), 80–82.
Myroshnychenko, V., Rodriguez-Fernandez, J., Pastoriza-Santos, I., Funston, A.M., Novo, C., Mulvaney, P., Liz-Marzan, L.M., de Abajo, F.J.G., 2008. Modelling the optical response of gold nanoparticles. Chemical Society Reviews 37, 1792–1805.
Nicewarner-Pena, S.R., Freeman, R.G., Reiss, B.D., He, L., Pena, D.J., Walton, I.D., Cromer, R., Keating, C.D., Natan, M.J., 2001. Submicrometer metallic barcodes. Science 294, 137–141.
Noguez, C., 2005. Optical properties of isolated and supported metal nanoparticles. Optical Materials 27 (7), 1204–1211 (Proceedings of the First Topical Meeting on Nanostructured Materials and Nanotechnology CIO 2004).
Oldenburg, S.J., Averitt, R.D., Westcott, S.L., Halas, N.J., 1998. Nanoengineering of optical resonances. Chemical Physics Letters 288, 243–247.
Oubre, C., Nordlander, P., 2004. Optical properties of metallodielectric nanostructures calculated using the finite difference time domain method. Journal of Physical Chemistry B 108, 17704–17747.
Ozbay, E., 2006. Plasmonics: merging photonics and electronics at nanoscale dimensions. Science 311, 189–193.
Palik, E.E., 1985. Handbook of Optical Constants of Solids. Academic Press, Orlando.
Park, H.S., Gall, K., Zimmerman, J.A., 2005. Shape memory and pseudoelasticity in metal nanowires. Physical Review Letters 95, 255504.
Pistol, M.E., Carlsson, N., Persson, C., Seifert, W., Samuelson, L., 1995. Observation of strain effects in semiconductor dots depending on cap layer thickness. Applied Physics Letters 67 (10), 1438–1440.
Purcell, E.M., Pennypacker, C.R., 1973. Scattering and absorption of light by nonspherical dielectric grains. Astrophysics Journal 1986, 705–714.
Qian, D., Liu, W.K., Zhang, Q., 2008. Concurrent quantum/continuum coupling analysis of nanostructures. Computer Methods in Applied Mechanics and Engineering 197, 3291–3323.
Qiu, L., Larson, T.A., Smith, D., Vitkin, E., Modell, M.D., Korgel, B.A., Sokolov, K.V., Hanlon, E.B., Itzkan, I., Perelman, L.T., 2008. Observation of plasmon line broadening in single gold nanorods. Applied Physics Letters 93, 153106.
Raschke, G., Brogl, S., Susha, A.S., Rogach, A.L., Klar, T.A., Feldmann, J., Fieres, B., Petkov, N., Bein, T., Nichtl, A., Kurzinger, K., 2004. Gold nanoshells improve single nanoparticle molecular sensors. Nano Letters 4 (10), 1853–1857.
Sambles, J.R., Bradbery, G.W., Yang, F., 1991. Optical excitation of surface plasmons: an introduction. Contemporary Physics 32 (3), 173–183.
Sershen, S.R., Westcott, S.L., Halas, N.J., West, J.L., 2002. Independent optically addressable nanoparticle-polymer optomechanical composites. Applied Physics Letters 80 (24), 4609–4611.
Sokolov, K., Follen, M., Aaron, J., Pavlova, I., Malpica, A., Lotan, R., Richards-Kortum, R., 2003. Real-time vital optical imaging of precancer using anti-epidermal growth factor receptor antibodies conjugated to gold nanoparticles. Cancer Research 63, 1999–2004.
Stone, J.W., Sisco, P.N., Goldsmith, E.C., Baxter, S.C., Murphy, C.J., 2007. Using gold nanorods to probe cell-induced collagen deformation. Nano Letters 7 (1), 116–119.
Sun, Y., Xia, Y., 2003. Gold and silver nanoparticles: a class of chromophores with colors tunable in the range from 400 to 750 nm. The Analyst 128, 686–691.
Wang, H., Tam, F., Grady, N.K., Halas, N.J., 2005. Cu nanoshells: effects of interband transitions on the nanoparticle plasmon resonance. The Journal of Physical Chemistry B 109, 18218–18222.
Weissleder, R., 2001. A clearer vision for *in vivo* imaging. Nature Biotechnology 19, 316–317.
Wokaun, A., Gordon, J.P., Liao, P.F., 1982. Radiation damping in surface-enhanced Raman scattering. Physical Review Letters 48 (14), 957–960.
Yee, K.S., 1966. Numerical solution of initial boundary value problems involving Maxwell's equations in isotropic media. IEEE Transactions on Antennas and Propagation 14 (3), 302–307.